

# Grain size dependence of dielectric properties of ultrafine BaTiO<sub>3</sub> prepared by a sol–crystal method

T. TAKEUCHI\*, M. TABUCHI, K. ADO, K. HONJO, O. NAKAMURA, H. KAGEYAMA

*Osaka National Research Institute, AIST, Ikeda, Osaka, 563 Japan*

Y. SUYAMA

*Shimane University, Matsue, Shimane, 690 Japan*

N. OHTORI

*Niigata University, Niigata, 950-21 Japan*

M. NAGASAWA

*Toyota Technological Institute, Nagoya, 468 Japan*

Ultrafine BaTiO<sub>3</sub> prepared by a decomposition of an organometallic crystal with unity of Ba/Ti ratio (sol–crystal method) has been characterized. While the as-prepared product resulting from the decomposition of the organometallic crystal at room temperature was BaTiO<sub>3</sub> with pseudo-cubic structure, the well-crystallized tetragonal polymorph was obtained by firing the as-prepared product above 1000 °C. Residual organic compounds, CO<sub>3</sub><sup>2-</sup> and OH<sup>-</sup> ions in the samples prevent the grain growth and tetragonal distortion of BaTiO<sub>3</sub>. We obtained quite higher room temperature permittivity (3700) at 1 kHz for the sample fired at 1200 °C than that (630) prepared by conventional solid-state reaction starting from BaCO<sub>3</sub> and TiO<sub>2</sub>. Such a high value was probably due to the accomplishment of homogeneous cation stoichiometry, which was achieved by this preparation method via the organometallic crystal with stoichiometric Ba/Ti ratio.

## 1. Introduction

Barium titanate (BaTiO<sub>3</sub>) is one of the most important materials in the electronics industry, particularly because of its high dielectric constant and ferroelectric properties [1]. Recently it has been widely studied for applications as a capacitor material in dynamic random access memory (DRAM) [2–5]. For DRAM applications in integrated circuits, thin film with both high dielectric constants and good insulating properties is required [5].

However, the dielectric constant of polycrystalline BaTiO<sub>3</sub> ceramics decreases for grain sizes below ~1000 nm [6, 7]. Furthermore, different crystallographic phases of this material appear, depending on the grain size; the ferroelectric tetragonal phase transforms to a paraelectric pseudocubic phase below ~100 nm at room temperature [8–11], although the tetragonal phase is stable in single crystals at room temperature. To explain these observations, we have analysed the X-ray diffraction profiles of the powder consisting of 100–1200 nm BaTiO<sub>3</sub> particles prepared by conventional solid-state reaction and by a hydrolysis method starting from Ba(OH)<sub>2</sub> and Ti[OCH(CH<sub>3</sub>)<sub>2</sub>]<sub>4</sub> and have found that the tetragonal

and cubic phases can coexist and that the relative amount of the cubic phase increases with decreasing particle size [12–14]. On the other hand, Asiaie *et al.* [15] investigated the grain structure of fine BaTiO<sub>3</sub> particles prepared by hydrothermal method using Raman spectroscopy and transmission electron microscopy (TEM) observations plus X-ray diffraction (XRD) measurements, and suggested the surface layer to be of tetragonal phase in which the long-range alignment of dipole moments was destructed by surface charge. We are aware of the possibility that the grain and crystal structures of fine BaTiO<sub>3</sub> particles depend on the preparation method, and also aware of the necessity of the sample characterization by combining TEM, scanning electron microscopy (SEM), XRD, infrared (i.r.) and Raman techniques.

In the present work, we have employed a method of a decomposition of an organometallic crystal (sol–crystal method) [16] to prepare ultrafine BaTiO<sub>3</sub>. This method has an important advantage as follows. Single crystals of metal alkoxides with Ba/Ti = 1 are synthesized from homogeneous mixing of both cations at temperatures <50 °C and then converted directly to the corresponding metal oxides

\* Author to whom correspondence should be addressed.

at room temperature. We believe that the organometallic crystal is one of the best precursor materials to prepare ultrafine BaTiO<sub>3</sub> particles, because the cation stoichiometry could be remained in the converted BaTiO<sub>3</sub> and the particle size is controllable by only post-heat treatment of the as-prepared BaTiO<sub>3</sub>. Such well-defined stoichiometry is seldom achieved for ultrafine particles prepared by solid-state reaction and sol-gel method [17]. The BaTiO<sub>3</sub> sample prepared by the sol-crystal method is suitable for investigating the particle size dependencies of both the crystal structure and dielectric property. We have tried to establish these relationships using fine BaTiO<sub>3</sub> particles obtained by the sol-crystal method.

## 2. Experimental procedure

BaTiO<sub>3</sub> particles were prepared by a sol-crystal method [16]. Guaranteed-reagent-grade barium metal (99.9% pure) was reacted with isopropyl alcohol (reagent grade) in a mixed solution of isopropyl alcohol and benzene (reagent grade) in which titanium tetraisopropoxide (Ti[OCH(CH<sub>3</sub>)<sub>2</sub>]<sub>4</sub>; reagent grade) was dissolved. All the solvents were dried with CaH<sub>2</sub> and distilled *in vacuo* prior to use. The reaction was conducted at 40 °C under an argon atmosphere with stirring until the barium metal was completely dissolved. The reaction vessel was stoppered and left at 5 °C, which led to crystal growth in the solution. The crystals were separated from the solution and dried in an argon atmosphere, which led to decomposition to a white powder (hereafter called the as-prepared sample). The as-prepared powder was fired at 650-, 800-, 1000- and 1200 °C for 4 h. The samples obtained were characterized by powder XRD (Rigaku RU-B), TEM (Hitachi H-300), SEM (Jeol JSM-T20), i.r. (Horiba FT-200) spectroscopy, Raman spectroscopy (Jobin Yvon T64000), thermogravimetry (TG; Rigaku TAS200), differential scanning calorimetry (DSC; Rigaku TAS200) and dielectric measurements (NF Electronic Instruments 2340-LCZ meter).

For electrical measurements, each powder was pressed into a pellet under a pressure of 30 MPa and was subsequently sintered in air for 2 h at the fired temperature. Gold paste was painted on both sides of the pellets, and they were fired at 600 °C for 20 min to form ohmic contact electrodes. Permittivity values at 1 kHz were measured using a three-probe method from 25 to 250 °C after moisture in the pellets was purged by N<sub>2</sub> flow at 300 °C.

## 3. Results and discussion

### 3.1. Sample morphology and content

The organometallic single crystals obtained were square, platelike in shape, and a few millimetres to 1 cm in size, as described elsewhere [16]. During exposure to air, the crystals converted to white powders with average particle diameters of 7 nm (as-prepared sample).

The powder XRD patterns (CuK<sub>α</sub> radiation) of the as-prepared, 800- and 1200 °C-fired samples are shown in Fig. 1. The main product is BaTiO<sub>3</sub>. Some amounts of BaCO<sub>3</sub> appear in the as-prepared sample and is

produced by reaction of the crystal with atmospheric carbon dioxide during the powder conversion process. BaCO<sub>3</sub> is also detected in i.r. spectra for the as-prepared and low-temperature-fired samples, as described below. This BaCO<sub>3</sub> would react with remaining amorphous TiO<sub>2</sub> to form BaTiO<sub>3</sub> after firing at high temperatures. With increasing firing temperatures, the intensity and sharpness of the BaTiO<sub>3</sub> peaks increase, indicating an increase in crystallinity and/or particle size. In fact, the crystallite size estimated from the full width at half maximum of the (1 1 1) and (2 2 2) peaks using Hall's method [18, 19] increases from 69 ± 7 to 180 ± 15 nm with increase in the firing temperature from 650 to 1200 °C. Also with increase in the firing temperature, peak splittings of the diffraction lines, such as (0 0 2) and (2 0 0), become clear, signifying the decrease in crystal symmetry of BaTiO<sub>3</sub> (i.e. a structural change from the cubic to tetragonal form). Detailed powder XRD analysis for each sample using CoK<sub>α</sub> radiation will be discussed later.

TEM micrographs of the as-prepared, 800 and 1200 °C-fired BaTiO<sub>3</sub> samples are shown in Fig. 2. In the as-prepared sample, primary particles with several nanometres cluster into agglomerates. These agglomerates grow into individual particles after firing at high temperatures (230 ± 50 nm for the sample fired at 1200 °C). This is consistent with the increase in crystallite size with increasing the firing temperature, as described above. Also SEM micrographs (Fig. 3) show the grain growth in the sintered BaTiO<sub>3</sub> samples. As seen in Fig. 3, the grain growth is almost suppressed by sintering below 800 °C, but steep increase in grain size is apparent above 1000 °C. Several authors have reported the decomposition and/or desorption of residual organic compounds and occluded water during the heating of BaTiO<sub>3</sub> prepared by wet-chemical processes [17, 20–22]. On the basis of these reports, we have characterized these species by i.r. and TG measurements.

Infrared spectra of the as-prepared and fired samples are shown in Fig. 4. The spectrum of the 1200 °C fired sample between 400 and 4000 cm<sup>-1</sup> exhibits only one absorption band around 550 cm<sup>-1</sup>. We assigned this band as normal vibrations of TiO<sub>6</sub> octahedron at

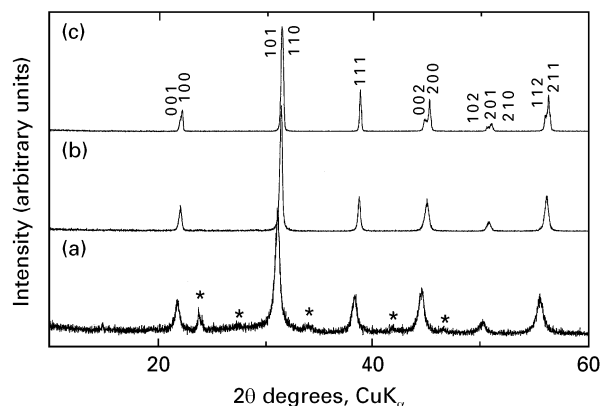


Figure 1 Powder X-ray diffraction patterns (CuK<sub>α</sub> radiation) for (a) as-prepared, (b) 800- and (c) 1200 °C-fired BaTiO<sub>3</sub> samples prepared by the sol-crystal method. Asterisk denotes peaks assigned to BaCO<sub>3</sub>.

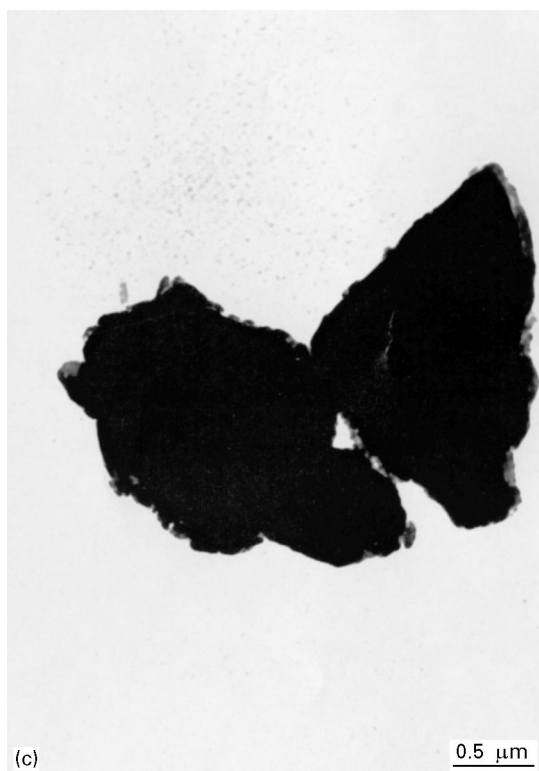
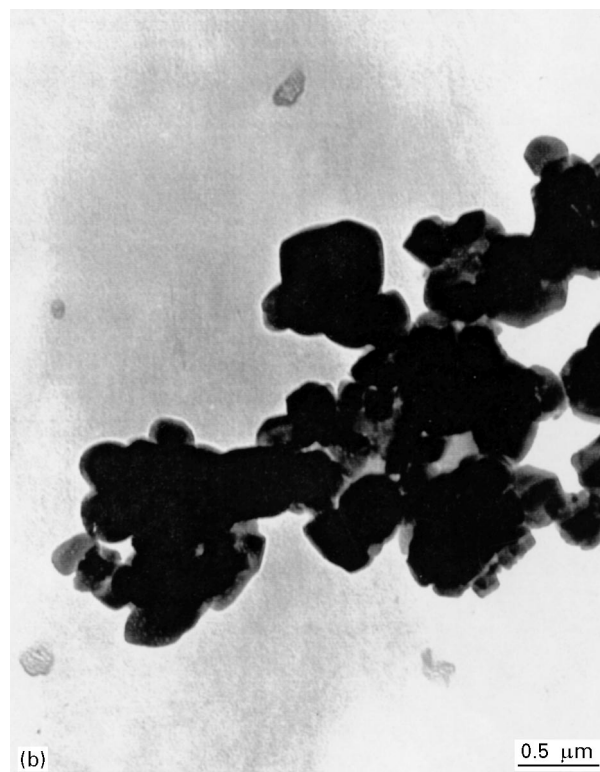
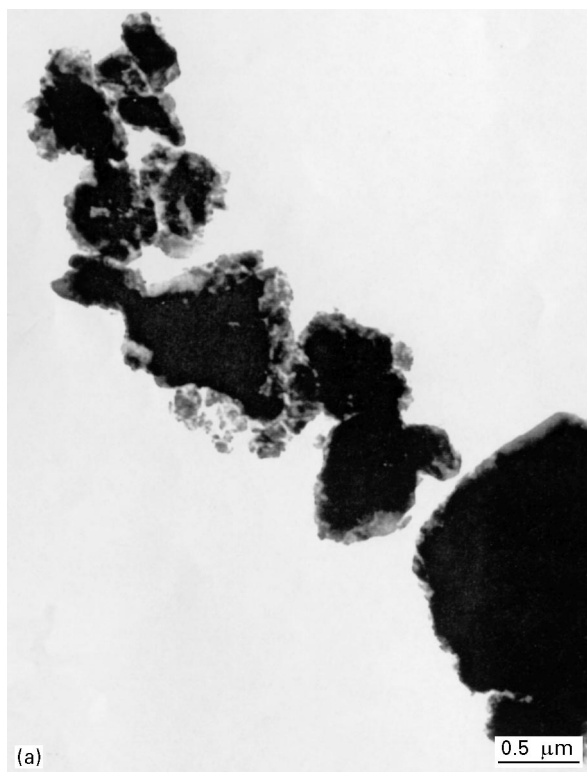


Figure 2 TEM micrographs for (a) as-prepared, (b)800- and (c) 1200 °C-fired BaTiO<sub>3</sub> samples prepared by the sol-crystal method. Magnification is the same for each micrograph.

540 and 630 cm<sup>-1</sup>, based on previous reports of BaTiO<sub>3</sub> powder [23, 24]. No detection of other absorption bands originating from impurities such as BaCO<sub>3</sub> and organic compounds reveals that the 1200 °C-fired sample consists of BaTiO<sub>3</sub> only. This is consistent with the result of XRD shown in Fig. 1. On the other hand, we found some additional absorption bands in i.r. spectra of the as-prepared sample and that fired below 1000 °C. We assigned these bands as vibrating and rotating modes originating from four different functional groups, that is, OH<sup>-</sup> (stretching at

3400 cm<sup>-1</sup>), H<sub>2</sub>O (stretching at 3400 cm<sup>-1</sup>, bending at 1600 cm<sup>-1</sup>, rotatory mode at 1050 cm<sup>-1</sup>), CO<sub>3</sub><sup>2-</sup> (stretching at 1430 cm<sup>-1</sup>, out-of-plane deformation at 856 cm<sup>-1</sup>) and CH groups (stretching at 2970 cm<sup>-1</sup>, deformation at 1350 cm<sup>-1</sup>). This assignment leads to the coexistence of BaCO<sub>3</sub>, some organic compounds and hydrated amorphous titania or occluded water with BaTiO<sub>3</sub> in the as-prepared sample, because the XRD pattern for the as-prepared sample shows the coexistence of BaCO<sub>3</sub> with BaTiO<sub>3</sub>, which was formed by the decomposition of organometallic crystal with Ba/Ti = 1. All these additional bands decrease their intensities with increasing firing temperature, indicating that these by-products were decomposed and/or desorbed up to 1200 °C. This tendency is shown in Fig. 5a, in which the intensity of each representative band, that is, deformation of CH at 1350 cm<sup>-1</sup>, stretching of OH<sup>-</sup> and H<sub>2</sub>O at 3400 cm<sup>-1</sup>, and stretching of CO at 1430 cm<sup>-1</sup>, was normalized by normal vibration of the TiO<sub>6</sub> octahedron. This result is supported by TG measurements, as shown in Fig. 5b. A continuous weight loss of about 9% was observed up to 1000 °C. Fig. 5a also shows the crystallite size ( $D_{hhh}$ ) described above as a function of firing temperature;  $D_{hhh}$  increases with firing temperature. Decomposition and/or desorption of residual organic compounds, water and BaCO<sub>3</sub> by firing therefore enhances the growth of both crystallites and particles of BaTiO<sub>3</sub>, especially above 900 °C, as visible in Fig. 3.

DSC measurements demonstrated the effect of residual organic compounds, water and BaCO<sub>3</sub> on the phase transition of BaTiO<sub>3</sub>. Fig. 6 presents DSC curves on heating around the Curie temperature for each sample. A phase transition between 124 and

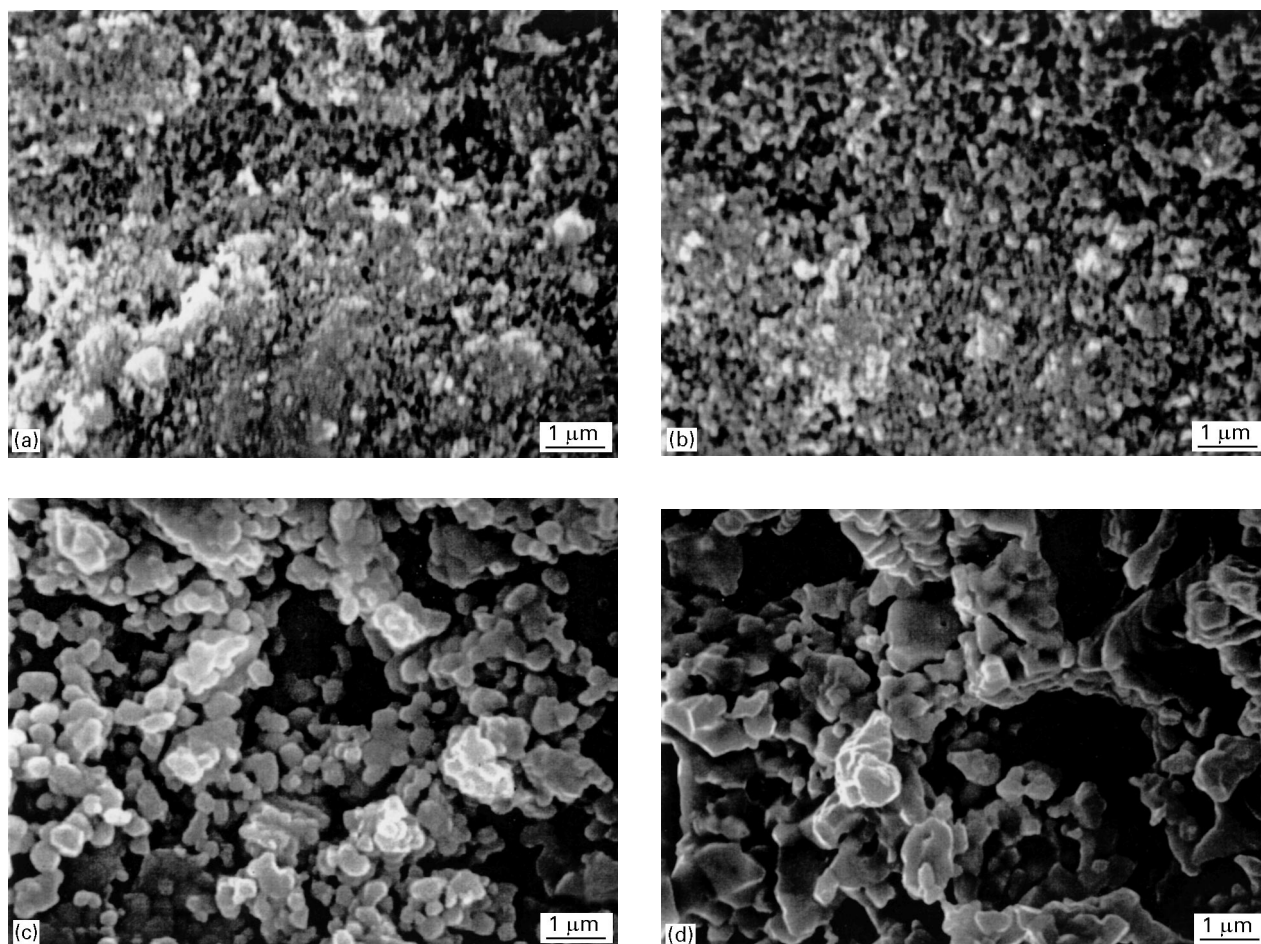


Figure 3 SEM micrographs for (a) 650-, (b) 800-, (c) 1000- and (d) 1200°C-fired BaTiO<sub>3</sub> samples prepared by the sol-crystal method.

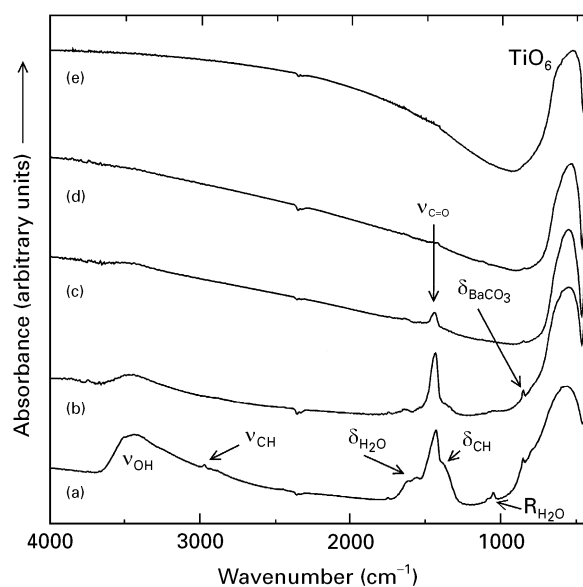


Figure 4 Infrared absorption spectra for (a) as-prepared, (b) 650-, (c) 800-, (d) 1000- and (e) 1200°C-fired BaTiO<sub>3</sub> samples prepared by the sol-crystal method. The band at 3400 cm<sup>-1</sup> is assigned as stretching of OH<sup>-</sup> (ν<sub>OH</sub>), at 2970 cm<sup>-1</sup> as stretching of CH groups (ν<sub>CH</sub>), at 1600 cm<sup>-1</sup> as bending of H<sub>2</sub>O (δ<sub>H<sub>2</sub>O</sub>), at 1430 cm<sup>-1</sup> as stretching of CO<sub>3</sub><sup>2-</sup> (ν<sub>C=O</sub>), at 1350 cm<sup>-1</sup> as deformation of CH groups (δ<sub>CH</sub>), at 1050 cm<sup>-1</sup> as rotatory mode of H<sub>2</sub>O (R<sub>H<sub>2</sub>O</sub>), at 856 cm<sup>-1</sup> as out-of-plane deformation of CO<sub>3</sub><sup>2-</sup> (δ<sub>BaCO<sub>3</sub></sub>), and at 550 cm<sup>-1</sup> as normal vibration of TiO<sub>6</sub>.

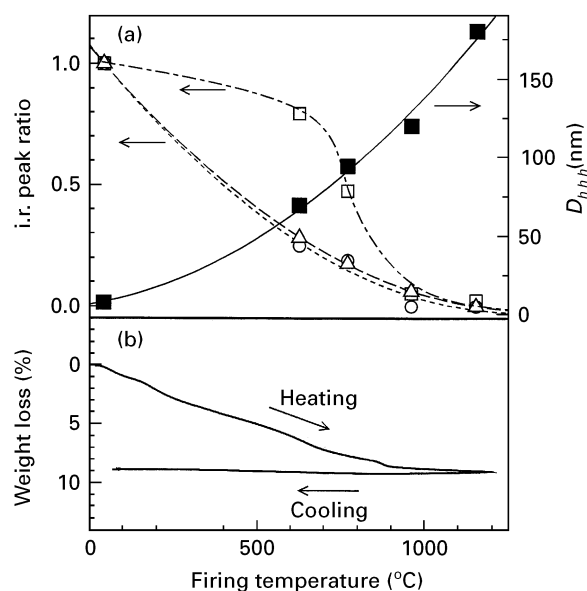


Figure 5 (a) Infrared peak intensity ratios of 1350 cm<sup>-1</sup> (deformation of CH; ○), 3400 cm<sup>-1</sup> (stretching of OH; △) and 1430 cm<sup>-1</sup> (stretching of CO; □) to that of 540 cm<sup>-1</sup> (vibration of TiO<sub>6</sub>) as a function of firing temperature. Each ratio is normalized to the as-prepared sample. Corresponding crystallite size ( $D_{h,hh}$ ) is also shown (■; see text). (b) Thermogravimetry of the BaTiO<sub>3</sub> sample prepared by the sol-crystal method.

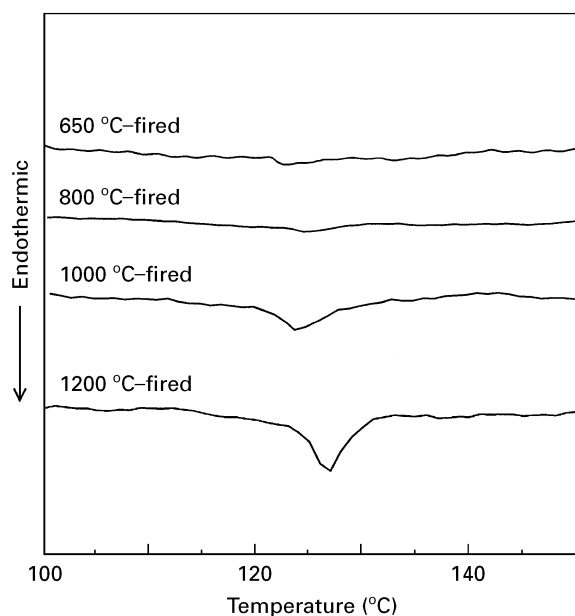


Figure 6 DSC traces for the 650-, 800-, 1000- and 1200 °C fired samples prepared by the sol-crystal method on heating. Heating rate is  $10\text{ }^{\circ}\text{C min}^{-1}$ .

$127\text{ }^{\circ}\text{C}$  is observed in the  $1200\text{ }^{\circ}\text{C}$ -fired sample. The enthalpy of this transition ( $\Delta H$ ), which was calibrated by that of  $\text{BaTiO}_3$  powder prepared by conventional solid-state reaction, is  $200\text{ J mol}^{-1}$ . This is consistent with previously reported values ( $209\text{ J mol}^{-1}$  [25]) for completely tetragonal  $\text{BaTiO}_3$ . In the  $1000\text{ }^{\circ}\text{C}$ -fired sample, the transition temperature lowers, and the corresponding  $\Delta H$  decreases. The 800- and  $650\text{ }^{\circ}\text{C}$ -fired samples showed a more diffuse and weaker endothermic peak around  $123\text{ }^{\circ}\text{C}$ . These results indicate that the relative amount of well-defined tetragonal phase increases with firing temperature, which is consistent with the change in crystal structure shown in Fig. 1. As described above, low-temperature fired samples contain some organic compounds, water and  $\text{BaCO}_3$ . Therefore, the decomposition and/or desorption of these species are related to the formation of well-defined tetragonal phase.

Thus we demonstrated that both particle and crystallite sizes of  $\text{BaTiO}_3$  prepared by the sol-crystal method could be controlled by firing condition. Simultaneously, the change in the crystal structure (pseudocubic to tetragonal unit cell) was observed by XRD measurements for samples fired at various temperatures, as shown in Fig. 1, which was supported by DSC measurements, as shown in Fig. 6. We expected that the change in the crystal symmetry and crystallite size of the samples would cause a dependence of the dielectric properties on the firing temperature. In the next section, the tetragonal content and the dielectric properties of the samples fired at different temperatures are examined in detail.

### 3.2. Relative amounts of tetragonal phase

For identification of both cubic and tetragonal phases and for determination of the relative amounts of tetragonal phase in the present  $\text{BaTiO}_3$ , we have analysed XRD peak profiles obtained by  $\text{CoK}_\alpha$  radiation.

The wavelength of  $\text{CoK}_\alpha$  ( $0.17890\text{ nm}$  for  $\text{K}_{\alpha_1}$ ) is longer than  $\text{CuK}_\alpha$  ( $0.15406\text{ nm}$ ), and provides higher resolution against  $2\theta$  in the diffraction profiles with relatively high intensities. For instance, the (002) peak of the tetragonal phase is located at  $2\theta = 52.594^{\circ}$ , whereas for the cubic phase it is located at  $2\theta = 52.833^{\circ}$ , on the basis of the lattice parameters previously described [1] and diffraction data [26]. The high resolution makes it possible to separate these two peaks, even considering line broadening in the small crystallite size region.

Fig. 7b, c and d show diffraction line profiles of the 800-, 1000 and  $1200\text{ }^{\circ}\text{C}$ -fired  $\text{BaTiO}_3$  samples around  $2\theta \sim 53^{\circ}$ . The observed diffraction profile was expressed by closed circles, and the calculated one was represented by solid lines corresponding to the superposition of each diffraction line consisting of  $\text{CoK}_{\alpha_1}$  and  $\text{CoK}_{\alpha_2}$  peaks. The diffraction profile of the as-prepared sample was more diffuse and less intensive (about 40 c.p.s.) than those of other three samples fired above  $800\text{ }^{\circ}\text{C}$ . Although we observed no apparent tetragonal distortion in the XRD profile for the as-prepared sample, we could not conclude whether the as-prepared sample is a single phase of cubic  $\text{BaTiO}_3$  or a mixture of cubic + tetragonal one because of the diffuse line profile. The peak profile of the  $800\text{ }^{\circ}\text{C}$ -fired sample exhibited asymmetry, which does not enable us to fit this profile by only one component. In addition, we observed obvious peak splittings for two samples fired above  $1000\text{ }^{\circ}\text{C}$ , suggesting the increase in tetragonal content with firing temperature. This is consistent with the increase of the enthalpy of transition with firing temperature, as described above (see Fig. 6). Then we analysed these peak profiles as consisting of three components; cubic (200) with lattice spacing of  $a = 0.4012\text{ nm}$  ( $\pm 0.0006\text{ nm}$ ), and tetragonal (200) and (002) with lattice spacing of  $a = 0.3997\text{ nm}$  ( $\pm 0.0006\text{ nm}$ ) and  $c = 0.4038\text{ nm}$  ( $\pm 0.0006\text{ nm}$ ). The tetragonal lattice spacings agree with those reported previously ( $a = 0.3994\text{ nm}$ ,  $c = 0.4038\text{ nm}$ ) [26], and the cubic lattice spacing agrees with a cube root of the tetragonal unit volume ( $a = 0.4009\text{ nm}$ ) [1]. Other peak profiles from  $2\theta = 10$  to  $90^{\circ}$  are also analysed in the same way. The tetragonal content is defined as the ratio of the integrated intensities of the tetragonal peaks to those of the total profile for each sample. The estimated tetragonal content increases with firing temperature. The formation of the tetragonal  $\text{BaTiO}_3$  in the  $1200\text{ }^{\circ}\text{C}$ -fired sample was also observed by Raman spectroscopy (Fig. 8).

The Raman spectrum indicates a distinct tetragonal structure in the  $1200\text{ }^{\circ}\text{C}$ -fired sample, as shown in Fig. 8a. This spectrum agrees well with that of the tetragonal  $\text{BaTiO}_3$  reported for single crystal and powder in the literature [27–31]; the bands around  $515$  and  $260\text{ cm}^{-1}$  are assigned to the transverse optical (TO) modes of  $A_1$  symmetry, whereas the sharp peak at  $305\text{ cm}^{-1}$ , which is characteristic of the tetragonal phase [27], is assigned to the  $B_1$  mode. The  $305\text{ cm}^{-1}$  peak reduces its sharpness and becomes indistinct in the as-prepared sample (Fig. 8b). This may indicate that the well-defined tetragonal structure is not remained in the as-prepared sample. As a refer-

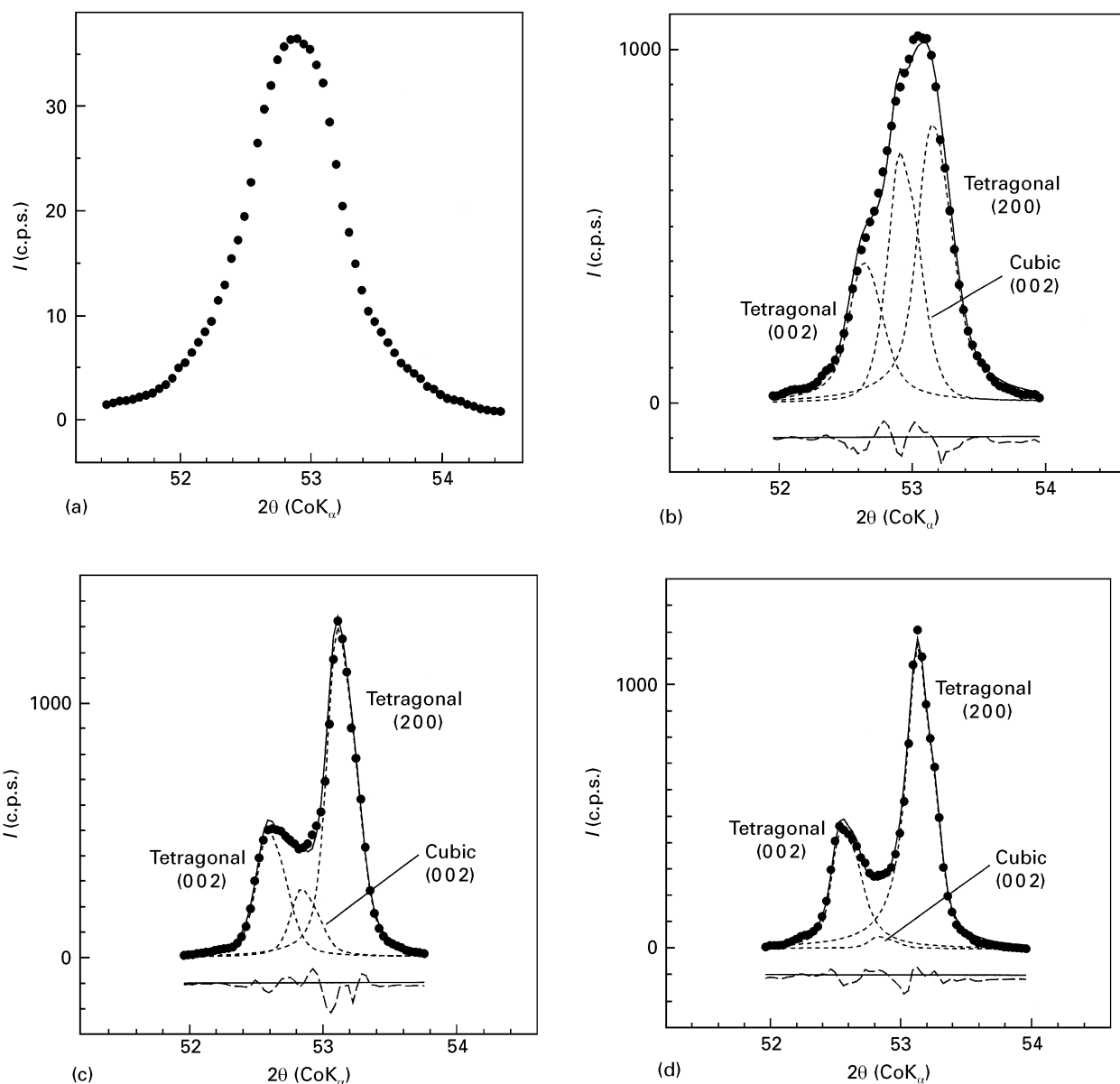


Figure 7 Powder X-ray diffraction line profiles ( $\text{CoK}_\alpha$  radiation) of (002) and (200) peaks ( $\bullet$  measured) for (a) as-prepared, (b) 800-, (c) 1000- and (d) 1200°C-fired  $\text{BaTiO}_3$  samples prepared by the sol-crystal method. Dashed lines are superpositions of each profile consisting of  $\text{K}_{\alpha_1}$  and  $\text{K}_{\alpha_2}$  peaks obtained by the best fit to a mixed Gaussian-Lorentzian distribution. (—) calculated line.

ence, the spectrum of cubic  $\text{BaTiO}_3$ , which was prepared by conventional solid-state reaction and measured at 150°C, is shown in Fig. 8c. Several authors reported that the  $305\text{ cm}^{-1}$  peak was detected even for fine particles and for thin films in their Raman spectra [15, 32–34], although their XRD profiles showed cubic symmetry. This discrepancy came from the difference of the sensitivity of both measurements; the structural information from the Raman spectra refers to single  $\text{TiO}_6$  octahedra, whereas the symmetry found by XRD is due to an ensemble of unit cells of more than  $10\text{ nm}^3$  [32]. Asiaie *et al.* [15] proposed a possible model for fine  $\text{BaTiO}_3$  particles that small domains with tetragonal structure distribute disorderly. In our as-prepared sample, the appearance of the  $305\text{ cm}^{-1}$  peak is not so obvious as to identify the crystallographic structure. The species such as organic compounds, occluded water and  $\text{BaCO}_3$  may interrupt the ordering of the tetragonal domains to lead to a pseudocubic phase in the as prepared sample, or

small domain size may force the unit cells to have pseudocubic symmetry.

The estimated fractions of the tetragonal component ( $[t]/\%$ ) are  $30 \pm 9$ ,  $64 \pm 10$ ,  $86 \pm 12$  and  $95 \pm 10$  for the 650-, 800-, 1000- and 1200°C fired samples, respectively. This tendency is consistent with the results of the enthalpy of transition ( $\Delta H$ ) described above. Fig. 9 shows  $\Delta H$  as a function of tetragonal content ( $[t]$ ), clearly indicating an increase in  $\Delta H$  with  $[t]$ . Again calorimetric measurement is demonstrated to give well-agreed results with XRD measurements. Fig. 10a shows  $[t]$  as a function of the crystallite size ( $D_{hh}$ ). The fraction of tetragonal component increases with crystallite size, indicating that the development of crystallite size probably accomplishes the transition from cubic to tetragonal phase or that disordered small domains in the pseudocubic phase probably align to form large tetragonal domains. As described above, thermal decomposition and/or desorption of impurities relates to the growth of the crystallite size

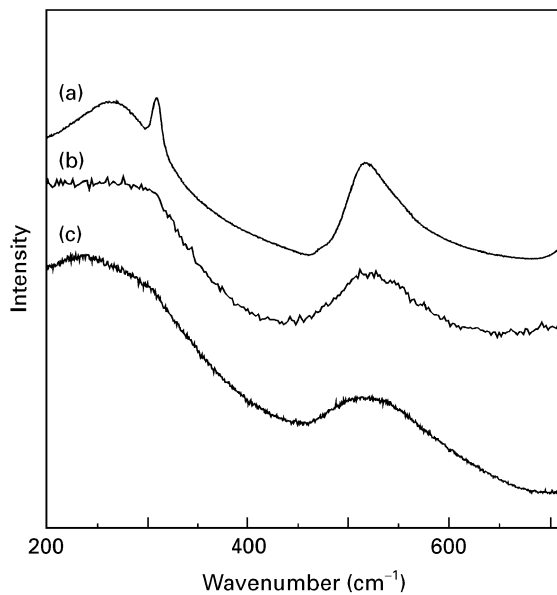


Figure 8 Raman spectra of (a) 1200°C-fired and (b) as-prepared BaTiO<sub>3</sub> samples prepared by the sol-crystal method. The spectrum of (c) cubic BaTiO<sub>3</sub>, which was prepared by conventional solid-state reaction and measured at 150°C, is also shown for reference.

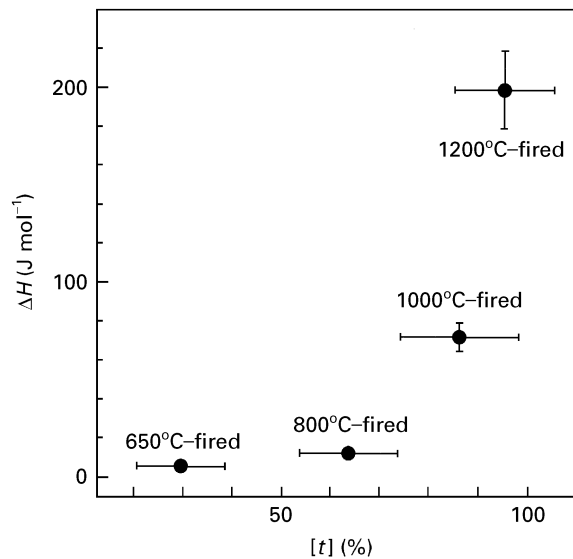


Figure 9 Enthalpy of transition ( $\Delta H$ ) at Curie temperature as a function of tetragonal content ( $[t]/\%$ ).

(see Fig. 5). Therefore, these impurities may suppress the phase transition from the cubic to tetragonal polymorph or may interrupt the ordering of the tetragonal domains in fine particles. Thus, by employing the sol-crystal method and CoK<sub>α</sub> XRD measurements, we were able to estimate the relative amounts of tetragonal and cubic phases for crystallite size below 200 nm.

Fig. 11 represents the variation of dielectric constant in the vicinity of the Curie temperature ( $T_C$ ), for samples fired above 800°C and that prepared by conventional solid-state reaction [12]. Relatively high dielectric constant at room temperature (more than five times) is achieved in the small particles (3700 for crystallite size  $D_{hhh} = 180$  nm) as compared with our

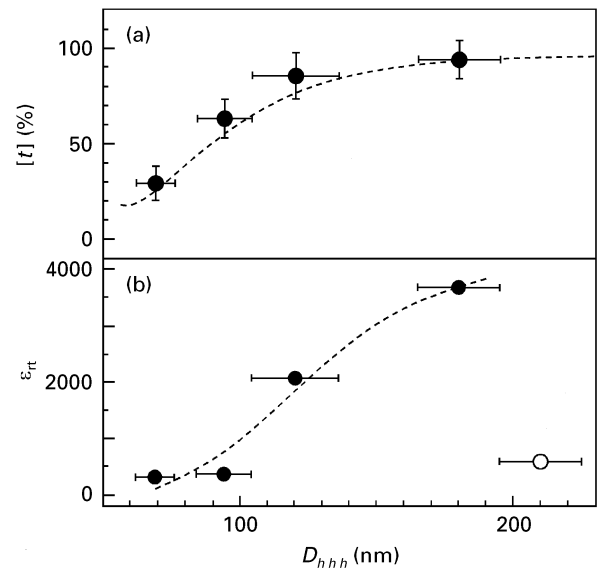


Figure 10 (a) Fraction of tetragonal content ( $[t]/\%$ ) as a function of crystallite size ( $D_{hhh}$ ). (b) The measured dielectric constants at room temperature ( $\epsilon_{rt}$ ) as a function of  $D_{hhh}$  (●). Data for BaTiO<sub>3</sub> prepared by conventional solid-state reaction [12] is also shown as (○).

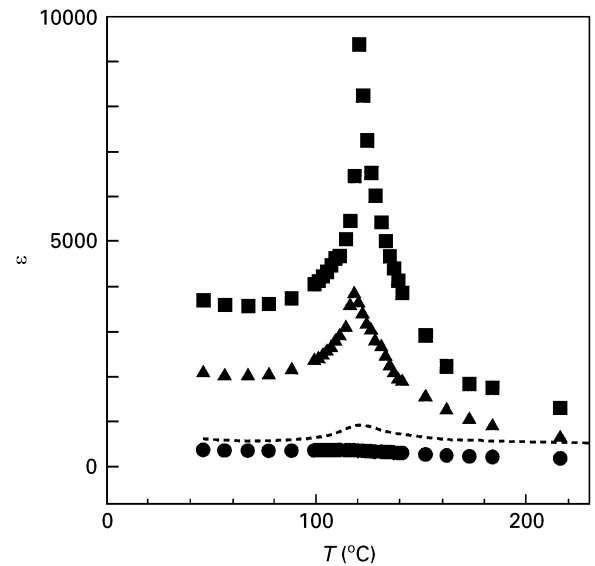


Figure 11 Measured dielectric constants as a function of temperature for BaTiO<sub>3</sub> prepared by the sol-crystal method. Data for BaTiO<sub>3</sub> prepared by conventional solid-state reaction [12] is also shown as a reference (---). (■) 1200°C-fired,  $D_{hhh} = 180$  nm; (▲) 1000°C-fired,  $D_{hhh} = 120$  nm; (---)  $D_{hhh} = 210$  nm; (●) 800°C-fired,  $D_{hhh} = 94$  nm.

previous samples prepared by conventional solid-state reaction (630 for  $D_{hhh} = 210$  nm) [12]. This may be due to the high homogeneity of the Ba<sup>2+</sup> and Ti<sup>4+</sup> cations in the precursor crystals accomplished by the sol-crystal method [16], as compared with that by solid-state reaction, because the BaTiO<sub>3</sub> prepared by solid-state reaction often shows heterogeneity of Ba/Ti ratio [17]. The low dielectric loss ( $\tan \delta = 0.02 \sim 0.03$ ) in the present samples suggests low oxygen defect concentrations. Fig. 11 reveals that the dielectric constant decreases and becomes nearly temperature independent with decreasing firing

temperature and crystallite size. For clarity, the relationship between dielectric constant at room temperature ( $\epsilon_{rt}$ ) and crystallite size ( $D_{hhh}$ ) is plotted in Fig. 10b. For reference, the value for BaTiO<sub>3</sub> prepared by conventional solid-state reaction [12] is also plotted as an open circle. With increasing the firing temperature (i.e. with increasing crystallite size, and simultaneously tetragonal content) the dielectric constant increases. This tendency agrees with the increase in the enthalpy of transition ( $\Delta H$ ) with firing temperature shown in Fig. 9; well-crystallized tetragonal domains are formed by high-temperature firing, leading to relatively high dielectric constant. Thus the results of dielectric measurements are consistent with the above relationships between tetragonal content and crystallite size and between enthalpy of transition and tetragonal content. The phase transition from the tetragonal to cubic polymorph or the alignment of the tetragonal domains would increase the dielectric constant with increasing the crystallite size. In the latter case, the dielectric behaviour for small grains resemble that of relaxors such as Pb(Mg<sub>1/3</sub>Nb<sub>2/3</sub>)O<sub>3</sub>, which have also randomly distributed domains and show a diffuse phase transition [35, 36].

Here we demonstrate the possibility to prepare sufficiently small-sized BaTiO<sub>3</sub> with high dielectric constant using the sol-crystal method, which will be applicable to a capacitor in a highly integrated circuit.

#### 4. Conclusions

We have investigated the crystallographic phases and dielectric properties of BaTiO<sub>3</sub> depending on the grain size, as prepared by decomposition of an organometallic crystals (sol-crystal method). The tetragonal content estimated increases from  $30 \pm 9$  to  $95 \pm 10\%$  with increasing the crystallite size ( $D_{hhh}$ ). The thermal decomposition of remaining organic compounds, water and BaCO<sub>3</sub> relates to the growth of the crystallites, which causes an increase in the dielectric constant. The measured dielectric constant at room temperature is relatively high: 3700 for  $D_{hhh} = 180$  nm sample, compared with that prepared by conventional solid-state reaction (630 for  $D_{hhh} = 210$  nm sample), which is probably due to the stoichiometry at the atomic level in the precursor crystal.

#### Acknowledgements

We wish to express our gratitude to Dr Derek C. Sinclair of the University of Aberdeen, UK for stimulating discussion.

#### References

1. J. NOWOTNY and M. REKAS, *Key Engng Mater.* **66/67** (1992) 45.
2. R. BACSA, P. RAVINDRANATHAN and J. P. DOUGHERTY, *J. Mater. Res.* **7** (1992) 423.

3. E. SHI, C. R. CHO, M. S. JANG, S. Y. JEONG and H. J. KIM, *ibid.* **9** (1994) 2914.
4. A. T. CHIEN, J. S. SPECK, F. F. LANGE, A. C. DAYKIN and C. G. LEVI, *ibid.* **10** (1995) 1784.
5. C.-R. CHO, E. SHI, M.-S. JANG, S.-Y. JEONG and S.-C. KIM, *Jpn J. Appl. Phys.* **33** (1994) 4984.
6. G. ARLT, D. HENNINGS and G. de WIT, *J. Appl. Phys.* **58** (1985) 1619.
7. D. HENNINGS, *Int. J. High Technol. Ceram.* **3** (1987) 91.
8. K. UCHINO, E. SADANAGA and T. HIROSE, *J. Amer. Ceram. Soc.* **72** (1989) 1555.
9. K. FUKAI, K. HIDAKA, M. AOKI and K. ABE, *Ceram. Int.* **16** (1990) 285.
10. T. YAMAMOTO, K. URABE and H. BANNO, *Jpn J. Appl. Phys.* **32** (1993) 4272.
11. K. SAEGUSA, E. R. WENDELL and H. K. BOWEN, *J. Amer. Ceram. Soc.* **76** (1993) 1505.
12. T. TAKEUCHI, K. ADO, T. ASAI, H. KAGEYAMA, Y. SAITO, C. MASQUELIER and O. NAKAMURA, *ibid.* **77** (1994) 1665.
13. T. TAKEUCHI, K. ADO, K. HONJO, H. KAGEYAMA, Y. SAITO, C. MASQUELIER and O. NAKAMURA, in "Solid State Ionic Materials", edited by B. V. R. Chowdari, M. Yahaya, I. A. Talib and M. M. Salleh (World Scientific Publishing Co., Singapore, 1994) p. 229.
14. T. TAKEUCHI, K. ADO, H. KAGEYAMA, K. HONJO, Y. SAITO, C. MASQUELIER and O. NAKAMURA, *J. Ceram. Soc. Jpn* **102** (1994) 1177.
15. R. ASIAIE, W. ZHU, S. A. AKBAR and P. K. DUTTA, *Chem. Mater.* **8** (1996) 226.
16. Y. SUYAMA and M. NAGASAWA, *J. Amer. Ceram. Soc.* **77** (1994) 603.
17. A. D. HILTON and R. FROST, *Key Engng Mater.* **66/67** (1992) 145.
18. W. H. HALL, *J. Inst. Met.* **75** (1950) 1127.
19. W. H. HALL, *Proc. Phys. Soc.* **A62** (1949) 741.
20. S. NAKA, F. NAKAKITA, Y. SUWA and M. INAGAKI, *Bull. Chem. Soc. Jpn*, **47** (1974) 1168.
21. M. STOCKENHUBER, H. MAYER and J. A. LERCHER, *J. Amer. Ceram. Soc.* **76** (1993) 1185.
22. T. TUNKASIRI and G. RUJIJANAGUL, *J. Mater. Sci. Lett.* **13** (1994) 165.
23. J. T. LAST, *Phys. Rev.* **105** (1957) 1740.
24. G. BUSCA, V. BUSCAGLIA, M. LEONI and P. NANNI, *Chem. Mater.* **6** (1994) 955.
25. G. SHIRANE and A. TAKEDA, *J. Phys. Soc. Jpn* **7** (1952) 1.
26. JCPDS Powder diffraction file, 5-626.
27. C. H. PERRY and D. B. HALL, *Phys. Rev. Lett.* **25** (1965) 700.
28. L. RIMAI, J. L. PARSONS, J. T. HICKMOTT and T. NAKAMURA, *Phys. Rev.* **168** (1968) 623.
29. M. DIDOMENICO, S. H. WEMPLE, S. P. S. PORTO and R. P. BAUMAN, *ibid.* **174** (1968) 522.
30. A. CHAVES, R. S. KATIYAR and S. P. S. PORTO, *ibid.* **B10** (1974) 3522.
31. J. JAVADPOUR and N. G. EROR, *J. Amer. Ceram. Soc.* **71** (1988) 206.
32. S. SCHLAG and H.-F. EICKE, *Solid State Commun.* **91** (1994) 883.
33. T. HAYASHI, N. OJI and H. MAIWA, *Jpn J. Appl. Phys.* **33** (1994) 5277.
34. G. BUSCA, V. BUSCAGLIA, M. LEONI and P. NANNI, *Chem. Mater.* **6** (1994) 955.
35. G. A. SMOLENSKII, V. A. ISUPOV, A. I. AGRANOVSKAYA and S. N. POPOV, *Sov. Phys. Solid State* **2** (1961) 2584.
36. T. TSURUMI, K. SOEJIMA, T. KAMIYA and M. DAIMON, *Jpn J. Appl. Phys.* **33** (1994) 1959.

Received 2 July 1996

and accepted 3 February 1997